

Teaching Robots to Build Simulations of Themselves

Authors: Yuhang Hu^{1*}, Jiong Lin¹, and Hod Lipson^{1, 2*}

Affiliations:

¹Creative Machines Laboratory, Mechanical Engineering Department, Columbia University, New York, NY 10027, USA

²Data Science Institute, Columbia University, New York, NY, 10027, USA

*Corresponding author. Email: yuhang.hu@columbia.edu, hod.lipson@columbia.edu

Abstract:

Simulation enables robots to plan and estimate the outcomes of prospective actions without the need to physically execute them. We introduce a self-supervised learning framework to enable robots model and predict their morphology, kinematics and motor control using only brief raw video data, eliminating the need for extensive real-world data collection and kinematic priors. By observing their own movements, akin to humans watching their reflection in a mirror, robots learn an ability to simulate themselves and predict their spatial motion for various tasks. Our results demonstrate that this self-learned simulation not only enables accurate motion planning but also allows the robot to detect abnormalities and recover from damage.

One-Sentence Summary:

A learning algorithm allows robots to model their own 3D kinematics and motor control from a 2D video for task planning.

Main Text:

INTRODUCTION

Every robot begins its life in simulation. Long before any robot is ever physically built, engineers meticulously design CAD models, craft kinematic equations, and estimate a variety of physical coefficients describing the robot to be. Using this simulation, the robot can be tested, programmed, and taught a variety of tasks. Only once this simulated robot meets intended performance, is it physically built and operated. Simulations remain essential for robot learning because learning in real life is slow, energetically expensive, and risky.

Humans and animals also use a simulator to learn. In contrast to robots, however, human and animal self-simulation is learned and evolved, not programmed by a designer. A child, for instance, creates a mental model of its own body by observing itself directly (or through a mirror reflection), refining its movements and gaining a deeper understanding of its body kinematics and motor control in relation to the environment. This morphological self-awareness and adaptability are what we aspire to instill in robots.

Body self-awareness, as demonstrated through mirror self-recognition, remains a unique cognitive ability reserved for only a few species, such as humans, chimpanzees, and orangutans. Most primates, despite prolonged exposure to mirrors, continue to perceive their reflection as another individual rather than recognizing it as an image of themselves [1, 2, 3]. This complex cognitive capacity to process mirrored information about oneself, which most primates seem to lack, raises pertinent questions about the nature of consciousness, the emergence of self-awareness, and its link to the development of the mind. In the human context, mirrors serve as instrumental tools for cognitive development, enhancing skills, refining gestures, and enabling a deeper understanding of one's body in relation to the surrounding environment. [4, 5].

Similarly, as robots become increasingly integrated into our daily routines, understanding their own 3D morphology is crucial for motion planning, navigation and preliminary robotic self-awareness [6, 7, 8, 9, 10]. This not only enables them to execute comprehensive planning tasks but also enhances their adaptability. Previous work in robotic self-modeling only focused on predicting the center of mass or the end-effector position of robots [11, 12]. Recent advancements in computational self-modeling have primarily leveraged several depth cameras to capture and predict a robot's kinematics [13]. The Neural 3D Visual Self-Model's groundbreaking potential highlights its pivotal role in 3D motion planning and control tasks. More than just a morphology prediction, this visual self-model exhibited handling damage detection, identification, and subsequent recovery for real-world robotic applications.

Our previous, however, work relied on five well-calibrated depth cameras, necessitating complex setups and intricate calibration processes. Furthermore, fusing multiple depth images from different devices into a coherent point cloud introduces noise and potential inaccuracies.

The question we aim to address in this paper is as follows: Can we teach robots to learn its body kinematics and morphology based on a single 2D camera, just as humans look into the mirror to learn without leveraging synthesized 3D ground truth data for supervision?

Enter Neural Radiance Fields (NeRF), a groundbreaking approach in Computer Vision [14, 15, 16, 17, 18, 19, 20, 21, 22]. NeRF models exploit volume rendering combined with explicit neural scene representation, trained through multi-view images devoid of 3D or depth supervisory information.

In this paper, we leverage such ability from NeRF to advance the boundaries of this research with a focus on modeling the robot's morphology and kinematics within a continuous 3D domain. We propose a self-supervised learning framework enabling robots to leverage videos for self-modeling, akin to a utilize mirrors to understand and refine their movements (Fig. 1A). We introduce Free Form Kinematic Self-Model which is a query-based model that can output the robot occupancy in 3D space (Fig. 1C). By keeping both the spatial coordinates and joint angles continuous, we can probe the robot's 3D morphology and kinematics with precision at any spatial location using any joint angles in action space. Besides, the model is fully differentiable, and we can search the robot motor commands using gradient-based optimization in real time. We also show how to use this model to perform basic manipulation tasks: 3D morphology prediction, motion planning without relying on kinematic equations, and abnormal detection alongside damage recovery (Fig. 1B). This approach's efficiency is evident in its compact size of 333 KB, a significant reduction from the previous work's 1.1 MB, showcasing its streamlined design and enhanced memory efficiency.

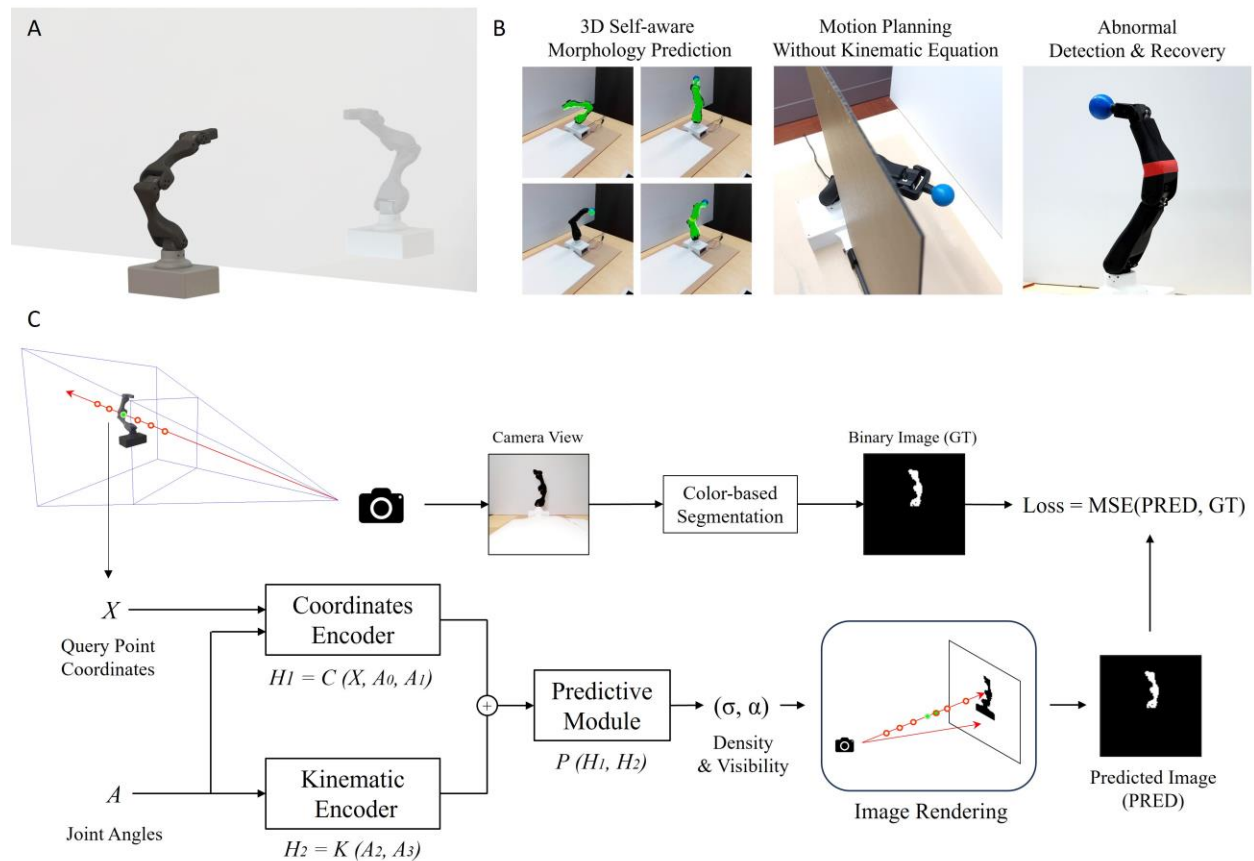


Fig. 1. Entire pipeline overview: (A) An illustrative representation of our foundational concept: a robot looking into a mirror, trying to build a model of itself by moving its body to observe changes. (B) Leveraging the model, the robot can predict its own morphology and perform a variety of manipulation tasks. (C) Free Form Kinematic Self-model representation. The model comprises three deep neural networks: a coordinates encoder, a kinematic encoder, and a predictive module. By processing 3D point coordinates and joint angles, it predicts the density and visibility of queried points. This information is then used to render a predicted image, which is compared with a segmented binary image for training.

Free-Form Kinematic Self-model

In the future autonomous robotics, it is increasingly important for robots that require minimal human supervision. Robots should learn to create models for themselves that not only generate motor commands to solve the problems but can adapt to changes and recovery from damage [23]. Engineers simplified the robot morphology and based on rigid body assumption to design a specific kinematic function for a robot [24]. To achieve morphology simulation for collision-free planning, it requires a detailed CAD model. In most simulations, the simple non-convex morphology, such as collision boxes is used to represent the robot morphology. As robots become more complex, manually modifying these functions when robot structures change becomes less feasible and less adaptable. For example, in instances where a robot sustains damage, the ability to quickly self-recover is also crucial.

To address these challenges, we introduce a visual self-supervised learning approach that allows the robot to autonomously learn a free form self-model including robotic kinematic and morphology from video. The free form kinematic self-model is a query-based deep neural networks trained by videos through motor babbling, so the model is task-agnostic and requires minimal human supervision. As depicted in Fig.1C, a robot is positioned within the camera view. By inputting specific 3D point location $X \in \mathbb{R}^3$, including the robot arm joint angles $A \in \mathbb{R}^4$, the model can predict whether the 3D point location is occupied by the robot and whether it is visible through the camera.

The free form kinematic self-model is composed of three deep neural networks: a coordinates encoder, a kinematic encoder, and a predictive module. The Coordinates Encoder takes in world coordinates X and the first two joint angles A_0, A_1 to compute a projection matrix T . This transformation produces virtual coordinates X' in which gives an equivalent effectiveness that the camera is the entity in motion and the first two robot arm joints are static. Then the virtual X' is fed into the Coordinates Encoder. Subsequently, the Kinematic Encoder processes the remaining joint angles. Concatenating the output of the Coordinates Encoder and the output from the Kinematic Encoder as input, the Predictive Module estimates the density σ and visibility α . The model can be expressed as:

$$(\sigma, \alpha) = P(C(T(X, A_0, A_1)), K(A_1, A_2))$$

To render a predicted image with length and width dimensions $W \times H$, we query M points in 3D space along the ray projected from the camera. The model generates the density and visibility for each point. The image rendering process aggregates the product of density and visibility values for every point along the projected ray. Considering all the M query points on each ray, the pixel value $Pred_{ij}$ at position (i, j) for the ray k , is:

$$Pred_{ij} = \sum_{k=1}^M \sigma_{ijk} \cdot \alpha_{ijk}$$

We use an RGB camera (Intel RealSense D435) to capture the video frames of the robot during motor babbling. We use a color-based segmentation method to convert the RGB frames into binary images that exclusively highlight the robot arm. The Mean Squared Error (MSE) between the model's predicted images and these binary images is utilized as the loss function to optimize the model's training. The loss function can be represented as:

$$\mathcal{L} = \frac{1}{W \times H} \sum_{i=1}^W \sum_{j=1}^H (Pred_{ij} - GT_{ij})^2$$

RESULTS

3D Morphology Predictions Using Free Form Kinematics Self-model

We conduct experiments both in the simulation and the real-world, using two 4 degrees of freedom robot arm. Figure 3A presents our real-world experimental setup. During data collection, the robot executes motor babbling. The camera saved the video frame once the motor encoder detects the joint angles met the motor commands. Each video frame is an RGB image, with a size of 100×100 . In the data collection phase (Movie S1), we collected a total of 12,000 data points. Among them, 10,000 are allocated for model training and validation at an 8:2 ratio, while the remaining 2,000 are for testing purposes.

In Fig.2 (B) we show the robot 3D morphology predictions obtained through the free-form kinematic self-model. The predicted results are shown as green points, while the robot ground truth morphology is shown in black. The green points in the 3D space stand for the queried points where the model estimate it is occupied by the robot. For every image, joint angles remained consistent, and sampled a volume of $100 \times 100 \times 64$ points to query the model about their respective densities. This process took 0.3 second on a desktop with a single GPU (NVIDIA GeForce RTX 3090). The first two rows present the results using Robot 1 hardware with simulation and real-world data. Pybullet serves as our chosen physical simulation platform. Lacking direct ground truth for the 3D morphology, we employ the CAD model of the actual robot for comparative reference [25]. Upon comparative analysis of the outcomes from the first and second rows, the results demonstrate a consistent performance, underscoring the robustness of our method in real-world scenarios. In the third row, we show that our model can effectively predict robot 2 morphologies which has different kinematics. This highlights the adaptability of our approach, making it suitable for diverse robots without the need for task-specific adjustments.

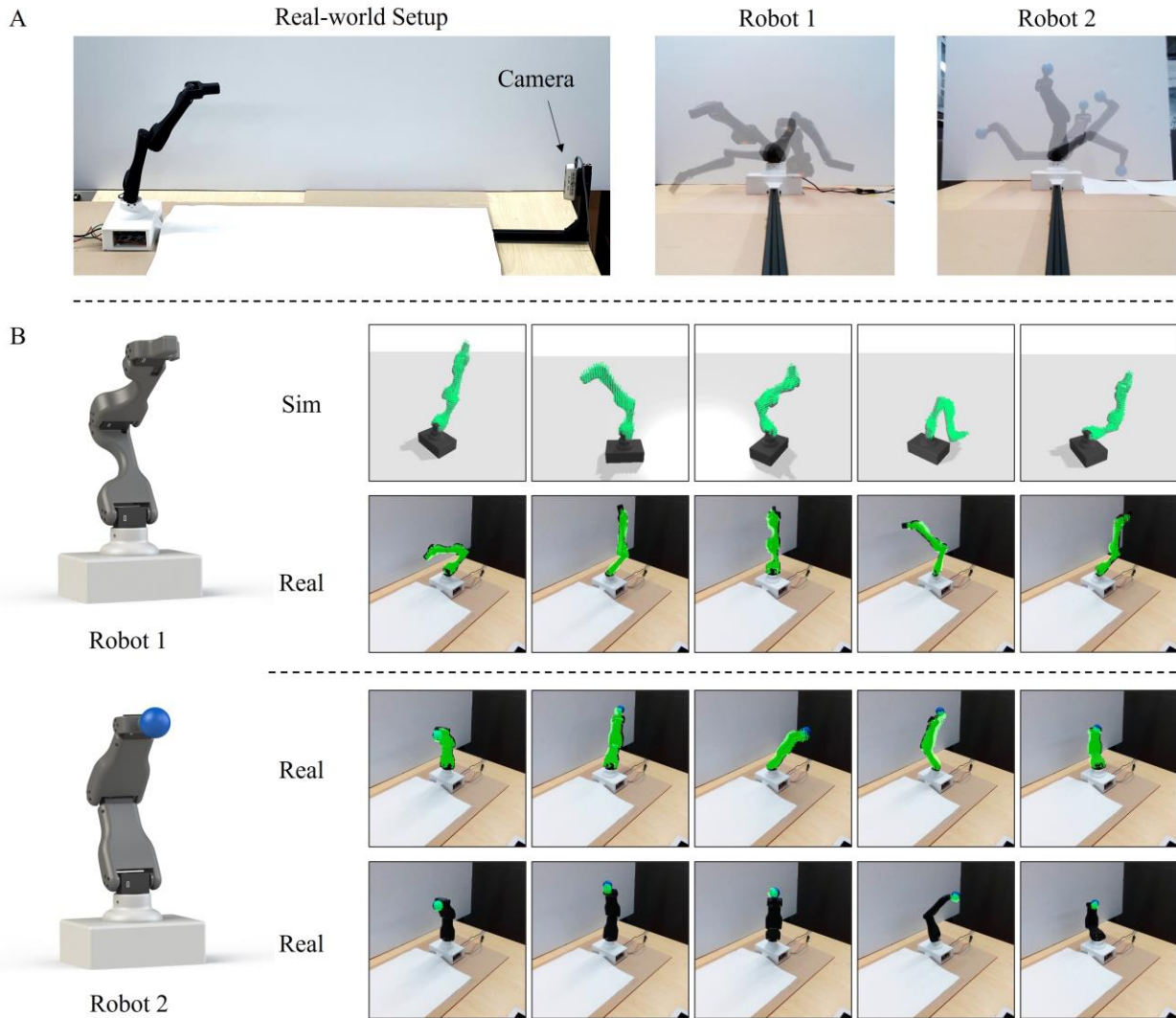


Fig. 2. Real-world experimental setup and 3D morphology prediction. (A) Real-world experimental setup. While the robot is doing motor babbling, the camera capturing its motion (left). The synthesized images represent typical captures by the camera (right). (B) Robot 1 and Robot 2 Hardware (left). On the right, predictions of robot 3D morphology using the free-form kinematic self-model are shown. The images demonstrate simulation and real-world predictions for both robots and the end-effector. Within each image, the actual robot is depicted in black, while predicted non-zero density areas are highlighted in green. Please see Movie S2 for more information.

Beyond predicting diverse robot morphologies, our model can also predict different components of a given robot. For example, to predict the end-effector of robot 2, we can achieve it through two training processes. During the first training phase, we train the model to predict the entire morphology of robot 2. Subsequently, we use video frames only that have the robot end-effector to fine-tune the model. Such images are procured by adjusting the color filter of the color-based segmentation module to isolate the blue pixels. The results demonstrate that our method can train models which have a capability to accurately predict robot occupancy in 3D space. This skill extends across different robots and even to specific robot components.

Motion Planning Using Free Form Kinematic Self-model

In this section, we illustrate how to use the trained model to achieve motion planning tasks. The FFKS can predict robot morphology in 3D space and also understand the specific component occupancy as we present in the previous section. Here we use robot 2 with a ball head end-effector to perform two manipulation tasks (Fig. 3).

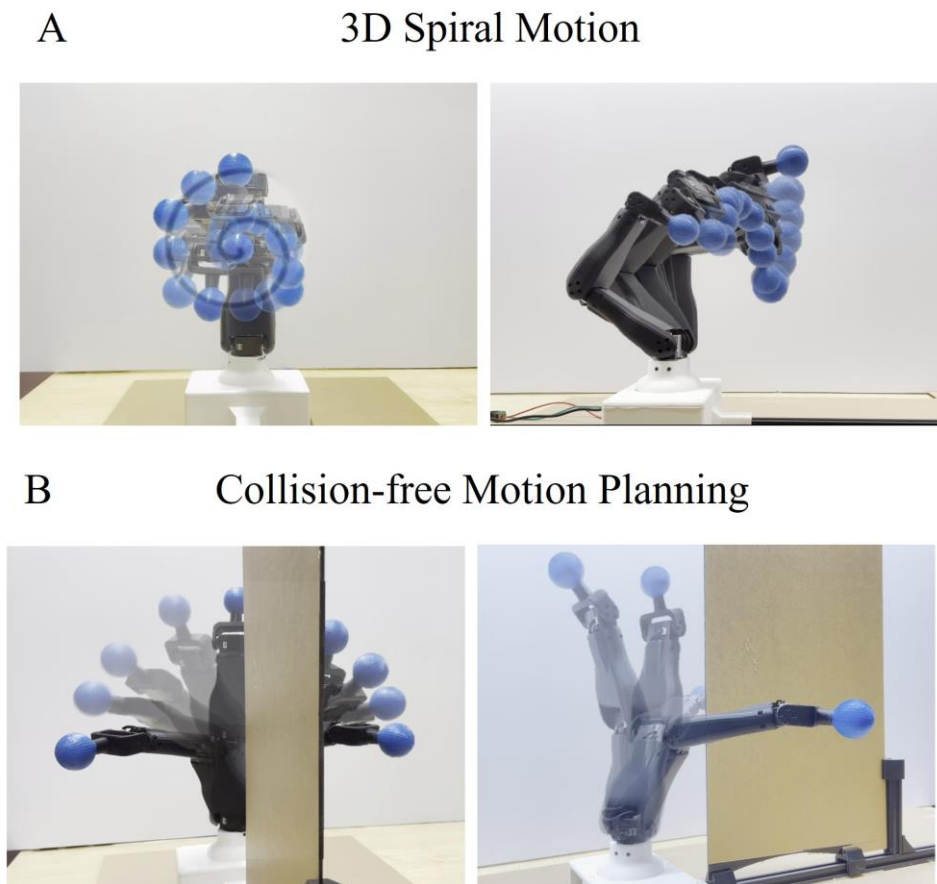


Fig. 3. Real Robot 2 performs motion planning tasks based on the Free Form Kinematic Self-model. (A) The robot tracks a 3D spiral trajectory. The images generated from a video illustrate the robot spiral trajectory. (B) The robot performs a collision-free motion planning task. The pictures show the robot's motion from a starting point to its target, navigating around obstacles to ensure no collisions.

The first task involves controlling the robot end-effector along a 3D spiral trajectory. This task is equivalent to performing Inverse Kinematic (IK) control, where the objective is to determine the joint angles based on the end-effector position. Traditional approaches would necessitate deriving equations rooted in the robot's mechanical geometries. In contrast, our method circumvents this necessity, permitting us to utilize gradient-based optimization to realize IK control. This is achieved without prior knowledge of the robot's hardware specifics or its Forward Kinematics (FK). Given that the 3D query points, joint angles, and our model are all differentiable, we present an algorithm that optimizes the joint angles by minimizing the distance between the predicted end-effector location and the target joint position.

To solve this problem, we use a model that is fine-tuned with end-effector data which can predict the 3D points occupied by end-effector. The end-effector position can be defined as the average

position of the query points with non-zero density. Assume Q is the set of all query points, and $Q_{occupied}$ is the subset of those points with non-zero density, i.e.,

$$Q_{occupied} = \{q \in Q | \sigma(q) > 0\}$$

Where σ is the density of query point as predicted by the model. Let θ represents the joint angles of the robot s.t.: $-90^\circ \leq \theta_i \leq 90^\circ$ for $i = 1, 2, 3, 4$. The end-effector position, p_{ee} , is the average position of all the points in $Q_{occupied}$:

$$p_{ee}(\theta) = \frac{1}{|Q_{occupied}|} \sum_{q \in Q_{occupied}} q$$

During the optimization process, we utilize the Adam optimizer for efficient convergence, with a learning rate set at 0.04 [26]. Backpropagation ensures iterative refinement of the joint angles by minimizing the Mean Squared Error (MSE) loss.

The second task is navigating the robot end-effector from a starting point to a target point without any collisions. We assume that the positions and dimensions of any obstacles in the robot's path are known a priori. Our approach leverages two FFKS models. The first predicts the entirety of the robot's morphology and is used for collision detection. The second predicts the position of the robot's end effector, serving as a heuristic calculator.

Through the model that can predict the whole-body morphology, the robot can estimate its body occupancy in a given configuration. A collision is deemed to occur if any portion of the robot's predicted morphology, represented by query points with non-zero density, intersects with the predefined obstacle region. To generate the robot collision-free trajectory, we use the Rapidly exploring random tree (RRT) algorithm [27]. RRT, known for its efficacy in high-dimensional spaces. The model predicting the end effector position, provides heuristics and guides the trajectory generation process. By leveraging two FFKSM, the robot can achieve collision-free motion planning. Please see Movie S3 for more information.

Abnormality Detection and Damage Recovery in the Real World

The versatility of the Free-Form Kinematic Self-Model extends beyond mere morphology prediction and motion planning. It can detect abnormalities and facilitate damage recovery. To illustrate this, consider a scenario where the robot faces an overload, leading to a bent in its link. To replicate this, we use 3D printing to fabricate the damaged component and integrate it with Robot 2 as shown in Fig. 5(A). This mechanical deformation induces a noticeable disparity between the images captured by the real camera and the 2D image predictions from the model, as seen in Fig. 4(B).

With the additional real-world data after the robot damage, the robot refines its predictions to align with the deformed 3D morphology. This adaptation is quantified in Fig.4 (C), which plots the decreasing divergence between the model's predictions and the ground truth as it is fine-tuned with the post-damage dataset. The plot shows the results from varied data quantities (10, 100, 1000 and 10000), demonstrating the model recovery effect at different data scales.

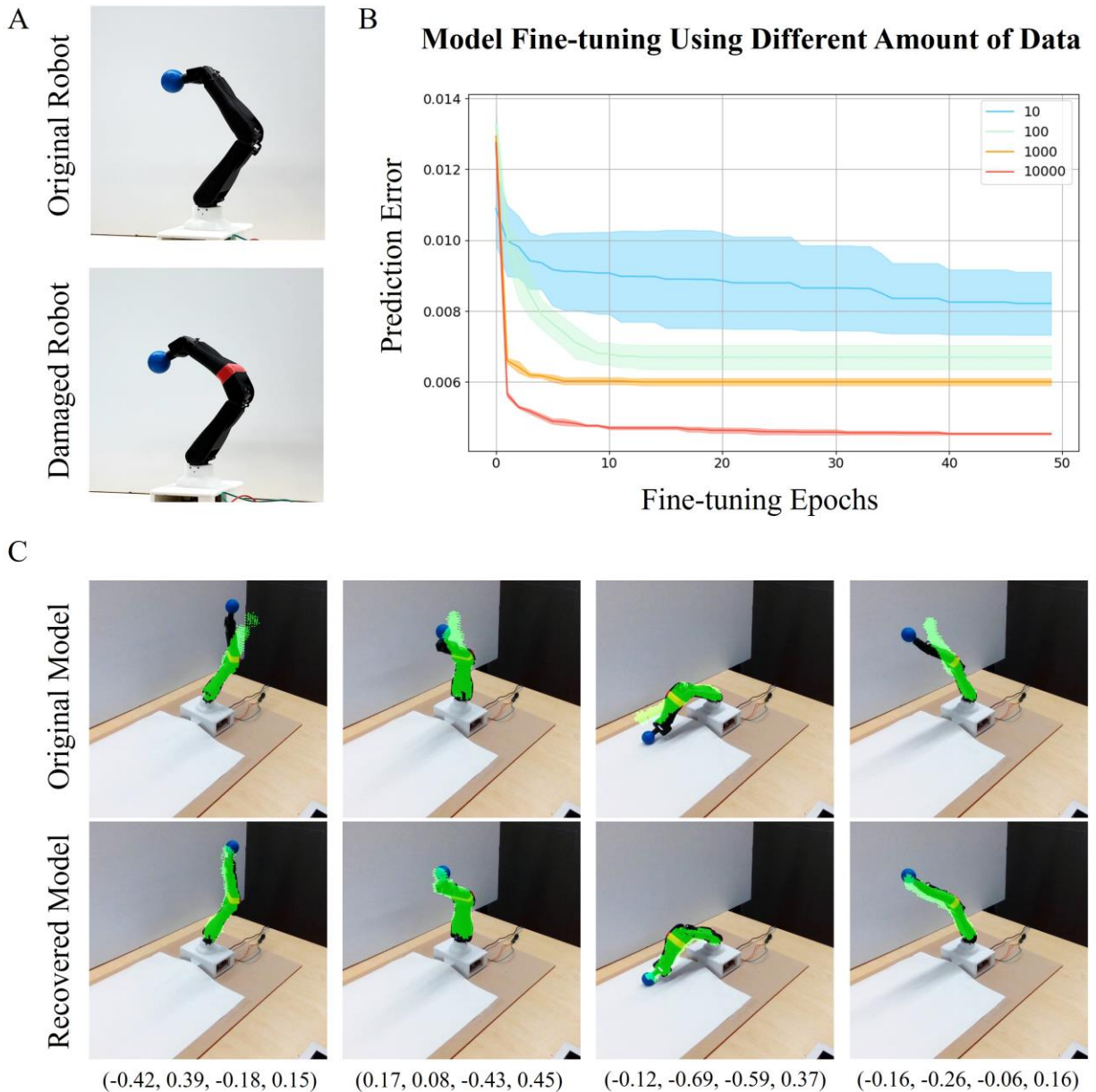


Fig. 4. (A) Real robot pictures for the experiments. (B) A plot indicating the divergence between the model's predictions and the ground truth during fine-tuning. (C) Prediction comparisons including the robot before retraining the model and after updating the model with post-damaged data.

Quantitative Evaluation of 2D Image Prediction

To assess the performance of our model, we use 2D predicted images, since directly measuring real-world 3D morphology without other sensors or equipment is unavailable. We use a test dataset comprising 2000 samples, unseen during the model training phase. Through querying 64 random points along each ray that spans robot space, our image rendering module can generate predicted images. The Mean Squared Error (MSE) serves as our metric to gauge the difference between these predictions and the ground truth.

Our experiments span three distinct configurations in a real-world environment: Full morphology prediction of Robot 1, Full morphology prediction of Robot 2, and Prediction of only the end-effector for Robot 2. We compare our method (OM) to the other two baseline methods. The first baseline, Random Selection (RS), arbitrarily picks an image from the training dataset. These randomly chosen images share a distribution similar to our test dataset, so we use this as one of our baselines. The second baseline, Nearest Neighbor (NN), chooses the image that has minimum L2 distance, in terms of joint angles, to the ground truth. The purpose of designing this baseline is that robotic arms with similar joint angles will have similar images from the camera view. Figure 5 shows that our method can accurately predict robot morphology and has lowest errors compared to the baselines across all tested configurations.

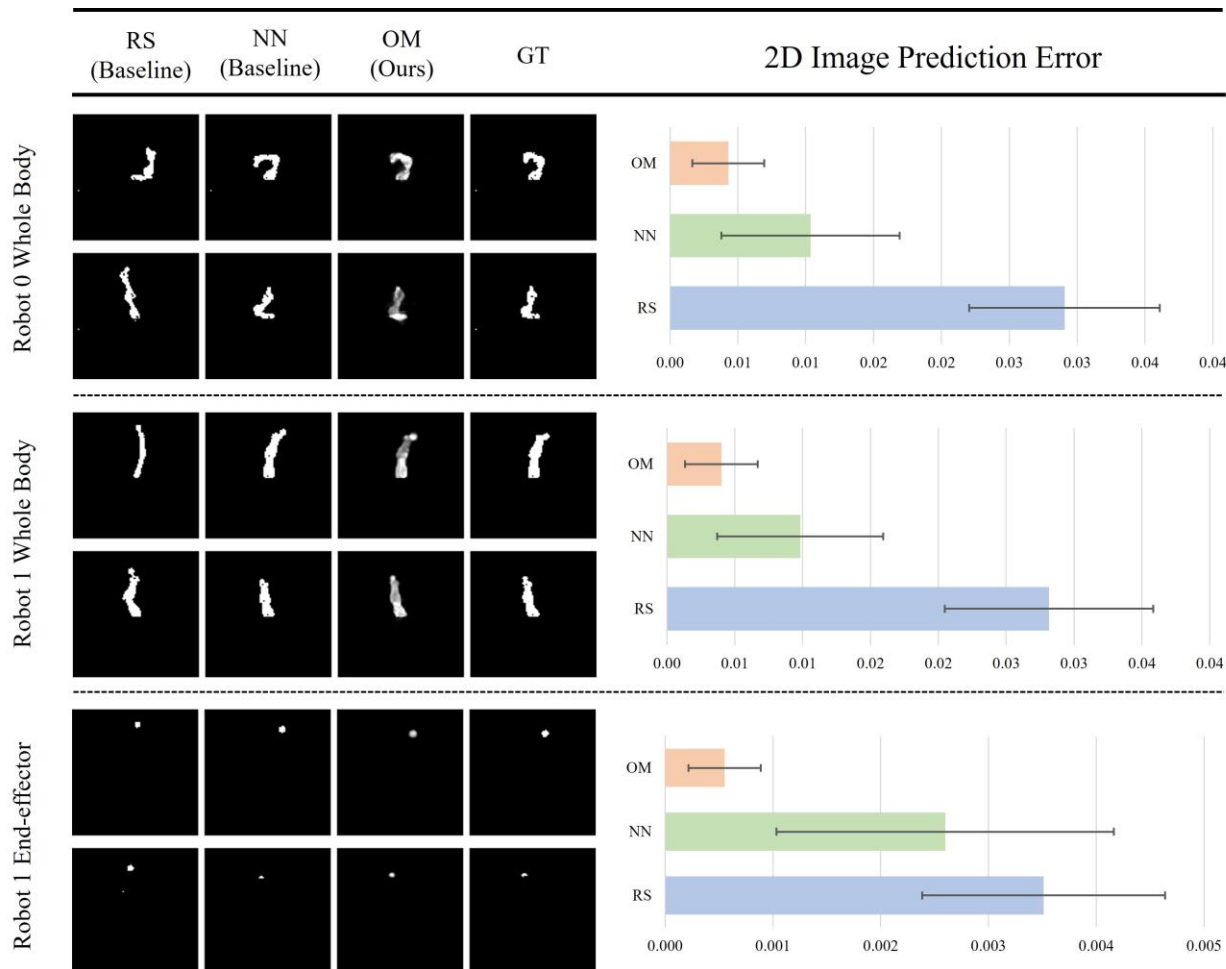


Fig. 5. Comparison of Predicted Robot Morphology and Quantitative Results. The left side presents a side-by-side comparison of the robot morphology predicted by baseline methods, our proposed method, and the ground truth, demonstrating the accuracy of our method in capturing the robot's shape. The right side showcases three bar plots illustrating quantitative results: our method consistently demonstrates lower prediction errors and standard deviations across all tests. The three tests, from top to down, represent predictions for robot 1 (whole body), robot 2 (whole body), and robot 2 (end-effector).

DISCUSSION

In summary, our experiments of 3D motion planning demonstrate the capability of the Free Form Kinematic Self-model (FFKSM) in addressing complex robotic manipulation tasks without the traditional reliance on kinematic functions or CAD models. Recent methods rely on intricate setups, necessitating the use of multiple depth cameras and laborious calibration processes to create ground truth for the model. However, our approach emphasizes the capability of a robot to self-model its morphology and kinematics through 2D visual feedback. This visual feedback loop is analogous to a human using a mirror, providing fast adaptation and resilience.

At the heart of our approach is the Free Form Kinematic Self-Model, a robot learning advancement that leverages the combination of deep learning and computer vision to build models for robots themselves. This approach not only facilitates morphology predictions and motion planning but also offers adaptability to a diverse range of robotic platforms. Our method bypasses the challenges encountered in manual modeling, particularly in cases where robots possess complex, evolving or damaged structures.

Through the experiments we demonstrated that our model has proficiently internalized the intricacies of robot kinematics and its 3D morphology. This foundational understanding can be harnessed effectively to navigate and address real-world challenges, setting a new paradigm in robotic motion planning and control.

Our key contributions can be summarized below:

1. **Robustness and Generalizability:** Our method displayed consistent performance in both simulated and real-world environments. This proves the robustness of the approach, making it reliable in varied contexts. Additionally, our approach could be extended across different robots through its generalizability.
2. **Versatility of Application:** Beyond mere kinematic modeling and morphology synthesizing, our method showcased its adaptability in abnormality detection and recovery processes. In real-world scenarios where robots may experience wear, tear, or damage, such a feature can recover the robot without human intervention.
3. **Tackling Motion Planning Tasks:** Traditional motion planning tasks, which rely on explicit kinematic equations and CAD-based modeling, can be computational-consuming and inflexible in dynamic environments. The FFKS method, through its gradient-based optimization and adaptability, provides an alternative approach that's both effective and efficient.
4. **Real-world Applicability:** A quintessential feature of our research was its emphasis on real-world applications. Whether it was in the prediction of morphologies, motion planning, or damage recovery, our approach consistently aligned with real-world scenario.

A potential limitation of our work, however, is the reliance on 2D images for quantitative evaluations. Given that direct measurements of real-world 3D morphology without auxiliary equipment is currently unattainable, our quantitative evaluation of 3D prediction is a compromise. In future research, enhancing the camera resolution and employing dynamic sampling techniques can substantially improve the model's accuracy. Additionally, integrating

3D modeling sensors could provide a comprehensive evaluation of the robot's kinematics and morphology.

In conclusion, the strides taken in this paper mark a significant progression in the domain of robotic self-modeling. The potential applications are vast, from autonomous robotics in industrial settings to those deployed in challenging terrains and environments. We believe that the principles laid out here will not only facilitate the rapid development and deployment of robotic solutions but also pave the way for robots that are more adaptive, resilient, and efficient.

REFERENCES

- [1] G. G. Gallup, "Self recognition in primates: A comparative approach to the bidirectional properties of consciousness.," *American psychologist*, vol. 32, p. 329, 1977.
- [2] G. G. Gallup Jr, J. R. Anderson and D. J. Shillito, "The mirror test," *The cognitive animal: Empirical and theoretical perspectives on animal cognition*, p. 325–333, 2002.
- [3] G. G. Gallup Jr, "Self-awareness and the emergence of mind in primates," *American Journal of Primatology*, vol. 2, p. 237–248, 1982.
- [4] T. F. Cash, *Body image.*, Oxford University Press, 2000.
- [5] H. J. Chiel and R. D. Beer, "The brain has a body: adaptive behavior emerges from interactions of nervous system, body and environment," *Trends in neurosciences*, vol. 20, p. 553–557, 1997.
- [6] W. Agnew, C. Xie, A. Walsman, O. Murad, Y. Wang, P. Domingos and S. Srinivasa, "Amodal 3d reconstruction for robotic manipulation via stability and connectivity," in *Conference on Robot Learning*, 2021.
- [7] W. Huang, C. Wang, R. Zhang, Y. Li, J. Wu and L. Fei-Fei, "Voxposer: Composable 3d value maps for robotic manipulation with language models," *arXiv preprint arXiv:2307.05973*, 2023.
- [8] C. Papachristos, S. Khattak, F. Mascariach, T. Dang and K. Alexis, "Autonomous aerial robotic exploration of subterranean environments relying on morphology-aware path planning," in *2019 International Conference on Unmanned Aircraft Systems (ICUAS)*, 2019.
- [9] Z. Xu, Z. He, J. Wu and S. Song, "Learning 3d dynamic scene representations for robot manipulation," *arXiv preprint arXiv:2011.01968*, 2020.
- [10] L. Steels and M. Spranger, "The robot in the mirror," *Connection Science*, vol. 20, p. 337–358, 2008.
- [11] R. Kwiatkowski and H. Lipson, "Task-agnostic self-modeling machines," *Science Robotics*, vol. 4, p. eaau9354, 2019.
- [12] R. Kwiatkowski, Y. Hu, B. Chen and H. Lipson, "On the Origins of Self-Modeling," *arXiv preprint arXiv:2209.02010*, 2022.
- [13] B. Chen, R. Kwiatkowski, C. Vondrick and H. Lipson, "Fully body visual self-modeling of robot morphologies," *Science Robotics*, vol. 7, p. eabn1944, 2022.
- [14] J. T. Barron, B. Mildenhall, M. Tancik, P. Hedman, R. Martin-Brualla and P. P. Srinivasan, "Mip-nerf: A multiscale representation for anti-aliasing neural radiance fields," in *Proceedings of the IEEE/CVF International Conference on Computer Vision*, 2021.
- [15] A. Pumarola, E. Corona, G. Pons-Moll and F. Moreno-Noguer, "D-nerf: Neural radiance fields for dynamic scenes," in *Proceedings of the IEEE/CVF Conference on Computer Vision and Pattern Recognition*, 2021.
- [16] C. Reiser, S. Peng, Y. Liao and A. Geiger, "Kilonerf: Speeding up neural radiance fields with thousands of tiny mlps," in *Proceedings of the IEEE/CVF International Conference on Computer Vision*, 2021.
- [17] Z. Wang, S. Wu, W. Xie, M. Chen and V. A. Prisacariu, "NeRF-: Neural radiance fields without known camera parameters," *arXiv preprint arXiv:2102.07064*, 2021.
- [18] B. Hu, J. Huang, Y. Liu, Y.-W. Tai and C.-K. Tang, "NeRF-RPN: A general framework for object detection in NeRFs," in *Proceedings of the IEEE/CVF Conference on Computer Vision and Pattern Recognition*, 2023.

- [19] V. Lazova, V. Guzov, K. Olszewski, S. Tulyakov and G. Pons-Moll, "Control-nerf: Editable feature volumes for scene rendering and manipulation," in *Proceedings of the IEEE/CVF Winter Conference on Applications of Computer Vision*, 2023.
- [20] C. Xu, B. Wu, J. Hou, S. Tsai, R. Li, J. Wang, W. Zhan, Z. He, P. Vajda, K. Keutzer and others, "Nerf-det: Learning geometry-aware volumetric representation for multi-view 3d object detection," in *Proceedings of the IEEE/CVF International Conference on Computer Vision*, 2023.
- [21] E. D. Zhong, T. Bepler, J. H. Davis and B. Berger, "Reconstructing continuous distributions of 3D protein structure from cryo-EM images," *arXiv preprint arXiv:1909.05215*, 2019.
- [22] J. Xu, L. Peng, H. Cheng, H. Li, W. Qian, K. Li, W. Wang and D. Cai, "Mononerf: Nerf-like representations for monocular 3d object detection," in *Proceedings of the IEEE/CVF International Conference on Computer Vision*, 2023.
- [23] J. Bongard, V. Zykov and H. Lipson, "Resilient machines through continuous self-modeling," *Science*, vol. 314, p. 1118–1121, 2006.
- [24] S. Kucuk and Z. Bingul, Robot kinematics: Forward and inverse kinematics, INTECH Open Access Publisher London, UK, 2006.
- [25] E. Coumans and Y. Bai, "Pybullet, a python module for physics simulation for games, robotics and machine learning," 2016.
- [26] D. P. Kingma and J. Ba, "Adam: A method for stochastic optimization," *arXiv preprint arXiv:1412.6980*, 2014.
- [27] S. La Valle, "Rapidly-exploring random trees: A new tool for path planning," *Research Report 9811*, 1998.
- [28] A. Paszke, S. Gross, F. Massa, A. Lerer, J. Bradbury, G. Chanan, T. Killeen, Z. Lin, N. Gimelshein, L. Antiga and others, "Pytorch: An imperative style, high-performance deep learning library," *Advances in neural information processing systems*, vol. 32, 2019.
- [29] A. F. Agarap, "Deep learning using rectified linear units (relu)," *arXiv preprint arXiv:1803.08375*, 2018.
- [30] M. Tancik, P. Srinivasan, B. Mildenhall, S. Fridovich-Keil, N. Raghavan, U. Singhal, R. Ramamoorthi, J. Barron and R. Ng, "Fourier features let networks learn high frequency functions in low dimensional domains," *Advances in Neural Information Processing Systems*, vol. 33, p. 7537–7547, 2020.
- [31] V. S. Ramachandran and W. Hirstein, "The perception of phantom limbs. The DO Hebb lecture.," *Brain: a journal of neurology*, vol. 121, p. 1603–1630, 1998.

Acknowledgments:

Funding:

This work was supported in part by the US National Science Foundation (NSF) AI Institute for Dynamical Systems (DynamicsAI.org), grant 2112085

Author contributions:

Yuhang Hu: Methodology (lead); Writing-original draft (lead); formal analysis (lead); Software (lead); Writing-review & editing (supporting); Conceptualization (equal); **Jiong Lin:** Methodology (supporting); Software (supporting); **Hod Lipson:** Writing-review & editing (lead); Conceptualization (equal); formal analysis (supporting)

Competing interests: Authors declare that they have no competing interests.

Data and materials availability: All data are available in the main text or the supplementary materials.

Supplementary Materials

Materials and Methods

Figs. S1

Movies S1 to S3

Data S1

Materials and Methods

Image rendering

To elucidate the rationale behind our model's dual output of α (density) and σ (visibility), consider the following: when viewing from the camera's perspective, only the robot's surface facing the camera influences image pixels. Given that we lack ground truth data for density and instead utilize 2D images for loss computation, purely relying on density for image rendering becomes untenable. Consequently, our model produces two outputs: the product of density and visibility determines the image rendering. If certain points are occupied by the robot but remain unseen, a visibility value of zero effectively nullifies density's contribution during image rendering.

Our methodology shares parallels with NeRF, which employs a neural network to depict a scene and synthesizes new views from sparse 2D imagery. Like NeRF, our approach learns 3D information from 2D images, integrating spatial points as pixels to guide the model. But, distinct from NeRF, our data collection relies on a stationary camera, with the robot's primary joints manipulated to emulate varied camera perspectives. Whereas NeRF generates four outputs (RGB and volume density), our emphasis centers on space occupancy. We explored the potential of adopting NeRF's volume rendering technique, questioning if a singular output—volume density—might suffice for our model. This approach, however, proved unsuccessful.

Further, incorporating the function $T(t)$ (representing the cumulative transmittance along a ray, i.e., the probability of a ray traveling from camera to the background without encountering any particle) did not yield better results. As depicted in Fig. S1, both attempts produced only black

images, underscoring that mere volume rendering and the accumulated transmittance function fall short in resolving this problem effectively.

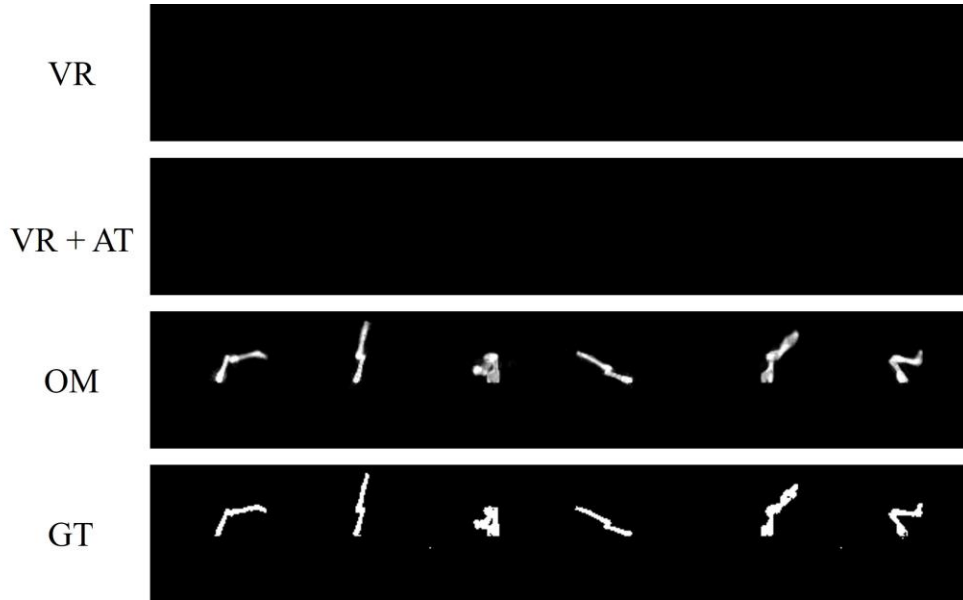


Fig. S1. Comparative Visualization of Different Methods versus Ground Truth. From top to bottom: (1) Volume Rendering method (VR) - yields a black image indicating ineffective learning, (2) Volume Rendering method with accumulated transmittance function (VR+AT) - similarly results in a black image, (3) Our method (OM) - shows accurate predictions, and (4) Ground truth (GT) for reference.

Model Architecture

The Free Form Kinematic Self-model is composite of three integral deep neural networks: the Coordinates Encoder, the Kinematic Encoder, and the Predictive Module. We implement them in Pytorch [28]. We use standard fully connected layers and use ReLU activation functions for all of them [29]. Before we input the coordinates and the joint angles into both encoders, we use Positional Encoding that enables the model to learn higher dimension data. Such an approach has been demonstrated to enhance the performance of Multi-Layer Perceptions [21, 30]. In our work, we use 5 frequencies, so the input dimension of Coordinates Encoder is mapped from 3 to 33 and that of Kinematic Encoder is mapped from 2 to 22.